Synthesis and Evaluation of In Vitro and In Vivo Trypanocidal Properties of a New Imidazole-Containing Nitrophthalazine Derivative

ARTICLE *in* EUROPEAN JOURNAL OF MEDICINAL CHEMISTRY · NOVEMBER 2015

Impact Factor: 3.45 · DOI: 10.1016/j.ejmech.2015.10.034

European Journal of Medicinal Chemistry 106 (2015) 106–119

Contents lists available at ScienceDirect

European Journal of Medicinal Chemistry

journal homepage: http://www.elsevier.com/locate/ejmech

Research paper

Synthesis and evaluation of *in vitro* and *in vivo* trypanocidal properties of a new imidazole-containing nitrophthalazine derivative

Francisco Olmo [a], Fernando Gómez-Contreras [b, **], Pilar Navarro [c], Clotilde Marín [a], María J.R. Yunta [b], Carmen Cano [b], Lucrecia Campayo [b], David Martín-Oliva [d], María José Rosales [a], Manuel Sánchez-Moreno [a, *]

[a] Departamento de Parasitología, Instituto de Investigación Biosanitaria, Hospitales Universitarios de Granada, Universidad de Granada, E-18071 Granada, Spain
[b] Departamento de Química Orgánica, Facultad de Química, Universidad Complutense, E-28040 Madrid, Spain
[c] Instituto de Química Médica, Centro de Química Orgánica M. Lora-Tamayo, CSIC, E-28006 Madrid, Spain
[d] Departamento de Biología Celular, Facultad de Ciencias, Universidad de Granada, Spain

ARTICLE INFO

Article history:
Received 6 July 2015
Received in revised form
18 October 2015
Accepted 20 October 2015
Available online 23 October 2015

Keywords:
Alkylaminonitrophthalazines
Imidazole
Trypanocidal activity
Chagas acute and chronic phases
Fe–SOD inhibition
Histopathological analysis

ABSTRACT

A series of new phthalazine derivatives (**1**–**4**) containing imidazole rings and functionalized with nitro groups in the benzene ring of the phthalazine moiety were prepared and identified on the basis of their MS, elemental analyses and bidimensional ^{1}H and ^{13}C NMR data, and their trypanocidal activity was tested. The 8-nitrosubstituted compound (**3**) was more active *in vitro* against *Trypanosoma cruzi* and less toxic against Vero cells than the reference drug benznidazole, and showed a SI value that was 47-fold better than the reference drug in amastigote forms. It also remarkably reduced the infectivity rate in Vero cells and decreased the reactivation of parasitemia in immunodeficient mice. Ultrastructural alterations found in epimastigotes treated with **3** confirmed extensive cytoplasm destruction in the parasites, whereas histopathological analysis of the hearts of mice infected and treated with **3** resulted in a decrease in cardiac damage. Biochemical markers showed that livers, hearts, and kidneys of treated mice were substantially unaffected by the administration of **3**, despite the presence of the potentially toxic nitro group. It was also found that this compound selectively inhibited the antioxidant parasite enzyme Fe–superoxide dismutase (Fe–SOD) in comparison with human CuZn–SOD, and molecular modeling suggested interaction with the H-bonding system of the iron-based moiety as a feasible mechanism of action against the enzyme.

1. Introduction

Trypanosomatid protozoa are the etiological agents of several major insect transmitted parasitic illnesses such as Chagas disease (*Trypanosoma cruzi*), sleeping sickness (*Trypanosoma brucei* subsp. *rhodesiense* and subsp. *gambiense*), and leishmaniasis (*Leishmania* spp.). These infections are concentrated in the poorest areas of the planet and are considered to be the three neglected tropical diseases (NTDs) with the highest rates of death [1]. Among them, Chagas disease is endemic in 21 Latin American countries and, although confined initially to the American continent, it is spreading to the rest of the world, owing to increased migration rates and different transmission modes, such as food, blood transfusions, organ transplants, and mother–newborn child infection [2]. Chagas disease has two phases: an acute stage, shortly after infection, and a chronic stage, developing over many years. The acute phase may have very mild, or even no, symptoms. After the acute phase, the disease goes into remission. Although the symptoms tend to resolve themselves, the infection persists if it is untreated. During the chronic phase, it may remain silent for decades, or even for life. However, about 30% of those infected develop life-threatening heart and/or digestive disorders, causing irreversible damage to the heart, esophagus, and colon [3].

Existing drug treatments for these diseases are far from satisfactory, and the development of a vaccine remains a goal to be achieved. Current therapies are not adequate, owing to several

* Corresponding author.
** Corresponding author.
E-mail addresses: fercon@ucm.es (F. Gómez-Contreras), msanchem@ugr.es (M. Sánchez-Moreno).

http://dx.doi.org/10.1016/j.ejmech.2015.10.034
0223-5234/

factors such as low therapeutic indexes, leading to high toxicities and unacceptable side effects, the emergence of resistant parasites, and difficulties in treatment compliance because of complex protocols and the high prices that are unaffordable for the affected countries [4]. These drawbacks of the current therapies make the search for new drugs an urgent requirement. Nevertheless, investment in the development of new drugs against these diseases is not financially attractive for pharmaceutical companies. In recent years, this bleak picture is changing, thanks to financial backing from nonprofit organizations and the involvement of public–private partnerships [5].

The main drugs currently used to treat Chagas disease are two nitroaromatic heterocycles: furane-based nifurtimox (NF) and imidazole-based benznidazole (BZN) [6]. Both drugs are effective in the acute phase of the disease, but their efficacy is low in the more challenging chronic phase [7], although BZN exhibits a better safety and efficacy profile than NF. Furthermore, these compounds have severe side effects including anorexia, vomiting, peripheral polyneuropathy, and allergic dermopathy [8]. The presence of nitro groups attached to heterocyclic rings suggests that these drugs act on the parasite through nitro reduction with the intermediation of neurotensin receptor (NTR) enzymes. Those reductions operate *via* nitroso and hydroxylamino intermediates, producing amines that modify biomolecules. However, the mode of action remains under discussion [9]. The high toxicity in humans is probably a result of oxidative or reductive tissue damage, which is inseparably linked to their antiparasitic activity [4].

Assuming the necessity of new antichagasic drugs, many research groups are involved in the design of molecules that are able to inhibit the performance of enzymes essential for parasite growth and survival [10]. In that context, one of the main self-defense strategies of *T. cruzi* is its highly active iron superoxide dismutase (Fe–SOD), which is an very efficient shield for preventing any oxidative damage from the host, in combination with peroxidases [11]. *T. cruzi* Fe–SOD is not present in mammals, which use CuZn–SOD or Mn–SOD for the same purpose, so that molecules acting selectively over Fe–SOD could be potential candidates for Chagas therapy [12]. On that basis, in previous work, we synthesized phthalazine and benzo[*g*]phthalazine derivatives containing imidazole rings linked to the pyridazine rings through flexible alkylamine arms (Fig. 1). Remarkably, most of those compounds were more active *in vitro* against *T. cruzi* and less toxic against mammal Vero cells than the reference drug BZN [13,14]. Furthermore, *in vivo* tests performed with the phthalazine derivatives on acute-phase Chagas disease gave parasitemia inhibition values better than those of BZN [14,15], and a decrease in the reactivation of parasitemia was found in the chronic phase for immunodeficient mice [14]. Interestingly, trypanocidal features are clearly structure-dependant, as the 1,4-bis(alkylamino) derivatives were always less active than their 1-alkylamino-4-chloro counterparts. Simultaneously, these heterocyclic systems inhibited the antioxidant parasite enzyme Fe–SOD, and the bis(alkylamino) derivatives were less effective inhibitors than their monoalkylamino analogs, so that a relationship between anti-*T. cruzi* activity and Fe–SOD inhibition was proposed by our group. Molecular modeling studies suggested that these highly complexing polyaminic heterocycles could affect Fe–SOD performance by interacting with the H-bonding amino-acid system of the iron-based moiety.

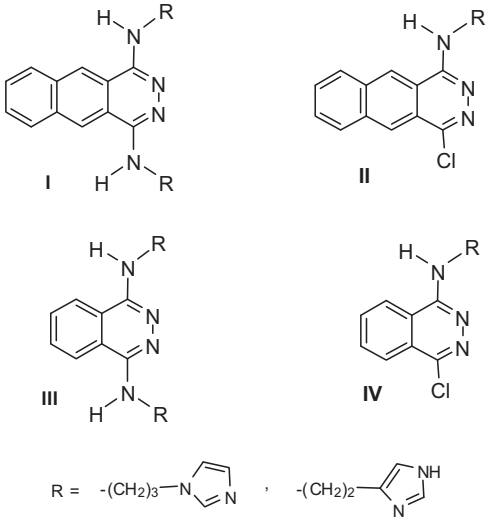

Fig. 1. Imidazole-containing benzo[g]phthalazine and phthalazine derivatives with potential antiparasitic activity.

Although the presence of a nitro group in a compound often (but not always) increases toxicity issues in the host, many nitroaromatic drugs have been used to treat parasitic infections, and compounds like nifurtimox, BZN, megazol, fexinidazole, and furaltadone are nitroheterocycles that specifically exhibit, as do other nitrocompounds, activity against *T. cruzi* and other trypanosomatids [16]. As noted above, their antiparasitic activity seems to be closely related to their ability to generate radical anions or reduced reactive species that increase oxidative stress in the parasite [17]. Many of the toxic effects observed after the administration of nitro drugs were found after prolonged treatment, but not with regimens of shorter duration. The potential of drugs like fexinidazole has encouraged researchers to further investigate the chemotherapeutic potential of nitro drugs for trypanosomatid diseases [18]. In this article, we report the antichagasic properties of a new series of imidazole-containing nitrophthalazine derivatives, in which the nitro group is located in two different positions with respect to the alkylamino side chain (Fig. 2). This allows us to evaluate whether different nitro locations also cause a structure–activity relationship and how is it related to Fe–SOD enzyme inhibition. We only deal with monoalkylamino-substituted compounds, as they have proved to be more active than their bis(alkylamino)-substituted analogs.

The antimicrobial properties were evaluated, first, *in vitro* against epimastigote, amastigote, and trypomastigote forms of *T. cruzi*, and Vero cells were used for the determination of unspecific cytotoxicity. The ability of the compounds to interfere with Fe–SOD was measured and structure–activity relationships were considered by performing molecular modeling of the enzyme–compound interaction. *In vivo* trypanocidal activities of the most active compounds were studied using a murine model from acute to chronic phases of Chagas, and the toxicity induced in the host was measured by analyzing different biochemical parameters in markers of the kidney, heart, and liver profiles. Ultrastructural alterations in parasites treated with the compound were investigated by transmission electron microscopy (TEM) in order to evaluate the damage caused.

2. Experimental section

2.1. Chemistry

The two starting imidazole-containing amines, 3-(imidazol-1-yl)propylamine and 2-(imidazol-4-yl)ethylamine (histamine), were purchased from Sigma–Aldrich and used without further purification. 3-Nitrophthalic acid was also obtained from Sigma–Aldrich. Solvents were dried using standard techniques [19]. 3-Nitrophthalic anhydride was prepared by refluxing 3-nitrophthalic acid in acetic anhydride for 1 h [20]. All of the

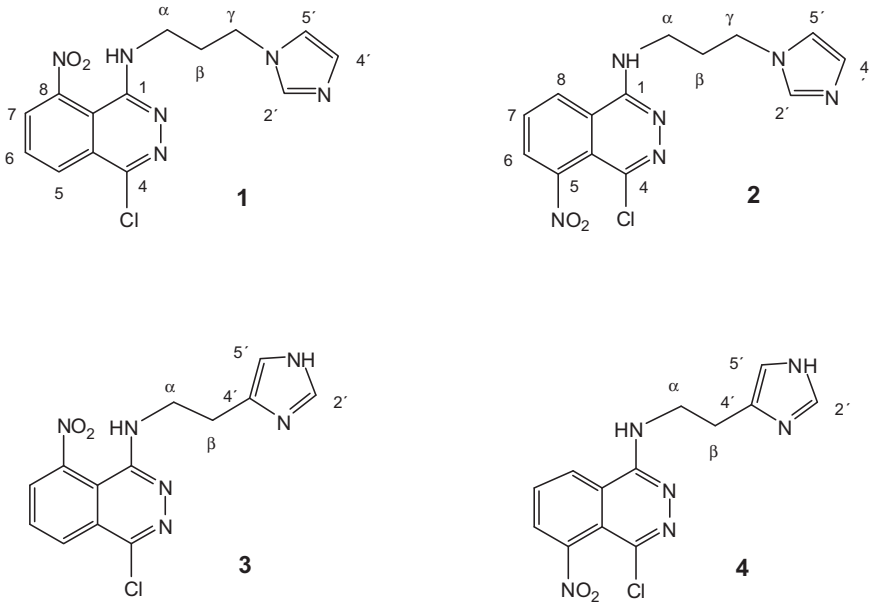

Fig. 2. Nitro-substituted phthalazine derivatives tested against *T. cruzi* in this study.

reactions were monitored using thin-layer chromatography (TLC) on precoated aluminum sheets of silica gel 60PF_{254} (Merck, layer thickness 0.2 mm). Compounds were detected using UV light (254 nm). Chromatographic separations were performed on columns in the indicated solvent system using flash chromatography on silica gel (particle size 0.040–0.063 mm). Melting points were determined in a Gallenkampf apparatus and were uncorrected. ^{1}H NMR spectra were recorded on a Bruker DPX 300 MHz and an AVIII at 700 MHz, whereas ^{13}C NMR spectra were recorded at 75 MHz at room temperature employing DMSO-d_6 as the solvent. Chemical shifts were reported in ppm (δ scale) from tetramethylsilane (TMS). All assignments were performed on the basis of ^{1}H–^{13}C heteronuclear single quantum coherence (gHSQC, spectra included in the Supplementary material file) and heteronuclear multiple-bond coherence (gHMBC) experiments. IR spectra were recorded on a Bruker alpha spectrometer with a DTGS detector at room temperature, furnished with ATR (attenuated total reflection), in the 7500–360 cm^{-1} range. Electrospray mass spectra were recorded with Bruker Esquire-LC apparatus. Elemental combustion analyses were performed in a Perkin–Elmer 2400-CHN instrument by the CAI of Microanalysis, Universidad Complutense, Madrid, Spain. Analyses indicated by the symbols of the elements or functions were within ±0.4% of the theoretical values and are shown in the Supplementary material file.

2.1.1. Synthesis of 5-nitrophthalhydrazide

The original synthesis described by Drew and Garwood [20] was modified as follows: 3-nitrophthalic anhydride (4 g, 0.02 mmol) was dissolved in boiling ethylene glycol (30 mL). After that, 80% hydrazine hydrate (1.04 g, 0.02 mmol) was added drop-wise and the mixture was refluxed for 1 h. When the resulting solution was cooled to room temperature, a yellow solid was formed. The precipitate was filtered to give 3.28 g (79%) of 5-nitrophthalhydrazide; mp > 300 °C. (*literature value* mp > 300 °C).[Beilstein 24,373]

2.1.2. Synthesis of 1,4-dichloro-5-nitrophthalazine

A solution of 5-nitrophthalhydrazide (1.0 g, 4.8 mmol) in phosphorous oxychloride (13 mL) and *N*,*N*-dimethylaniline (1.2 mL) was heated at 110 °C for 1 h. After cooling to room temperature, the solvent was evaporated under vacuum and the obtained residue was poured into ice and the mixture was stirred at 0–15 °C until a crystalline solid was formed. The precipitate was filtered, washed with cold water, dried *in vacuo*, and purified by flash column chromatography (toluene/ethyl acetate, v/v: 2/1). The fraction of R_f = 0.53 afforded 580 mg of a solid, which was identified as the title compound (50% yield), mp 176–178 °C. IR (KBr) ν_{max} = 3109, 2925, 2856, 1643, 1574, 1517, 758 cm^{-1}. ^{1}H NMR (DMSO-d_6) δ: 8.71 (d, 1H, J = 8.7 Hz, H-6), 8.68 (d, 1H, J = 8.7 Hz, H-8), 8.42 (t, 1H, H-7) ppm. ^{13}C NMR (DMSO-d_6): δ 154.8 (C-1), 148.8 (C-4), 145.0 (C-7), 135.6 (C-5), 130.2 (C-6), 129.8 (C-8), 127.7 (C-8a), 117.7 (C-4a) ppm. MS-ESI (MeOH): *m*/*z* (%), 243 (MH^+, 43), 225 (11), 157 (100).

2.1.3. Synthesis of **1** and **2** (method A)

A solution of 1,4-dichloro-5-nitrophthalazine (0.952 g, 3.9 mmol), 3-(imidazol-1-yl)propylamine (0.976 g, 7.8 mmol), and triethylamine (2 mL) in toluene (20 mL) was heated at 85 °C for 2 h. After cooling to room temperature, the solvent was removed under reduced pressure. The residue was purified by flash column chromatography (toluene/ethyl acetate/ethanol, v/v: 0.5/1/0.5). The appropriate fractions (monitored by TLC with the same eluent mixture composition) were combined to give three alkylamination products. The fraction with R_f = 0.45 was discarded as an hydroxilated subproduct. The fraction with R_f = 0.56 afforded 195 mg (15% yield) of an orange solid, which was identified as 1-[3-(imidazol-1-yl)propylamino]-4-chloro-8-nitrophthalazine (**1**), mp 164–165 °C. IR (KBr) ν_{max}: 3417, 2937, 1645, 1534, 1513, 1302, 1081 cm^{-1}. ^{1}H NMR (DMSO-d_6) δ: 8.54 (d, 1H, J = 7.6 Hz, H-7), 8.43 (d, 1H, J = 8.3 Hz, H-5), 8.17 (t, 1H, J = 8.0 Hz, H-6), 7.64 (s, 1H, H-2′), 7.20 (s, 1H, H-5′), 6.90 (s, 1H, H-4′), 6.79 (t, 1H, J = 5.1 Hz, NH-C1), 4.08 (t, 2H, J = 6.9 Hz, Hγ), 3.41 (m, 2H, Hα), 2.09 (m, 2H Hβ).^{13}C NMR (DMSO-d_6) δ: 151.34 (C-1), 146.23 (C-8), 144.41 (C-4), 137.73 (C-2′), 133.60 (C-6), 130.16 (C-7), 129.97(C-5), 128.85 (C-4′), 127.46 (C-4a), 119.78 (C-5′), 111.32 (C-8a), 44.23 (Cγ), 39.41 (Cα), 29.86 (Cβ). MS-ESI (MeOH) *m*/*z* (%): 333 (MH^+, 100). Anal. $C_{14}H_{13}ClN_6O_2$ (C, H, N). The fraction with R_f = 0.20 afforded 275 mg (21% yield) of a yellow solid which was identified as 1-[3-(imidazol-1-yl)propylamino]-4-chloro-5-nitrophthalazine (**2**), mp > 211 °C (dec). IR (KBr) ν_{max}: 3280, 2954, 1654, 1539, 1519, 1015 cm^{-1}. ^{1}H NMR

(DMSO-d_6) δ: 8.62 (d, 1H, J = 8.0 Hz H-6), 8.41 (d, 1H, J = 7.5 Hz, H-8), 8.16 (t, 1H, J = 8.1 Hz, H-7), 8.09 (t, 1H, J = 5.1 Hz, NH-C1), 7.76 (s, 1H, H-2′), 7.26 (s, 1H, H-5′), 6.94 (s, 1H, H-4′), 4.12 (t, 2H, J = 6.9 Hz, Hγ), 3.54 (m, 2H, Hα), 2.15 (m, 2H Hβ).^{13}C NMR (DMSO-d_6) δ: 153.72 (C-1), 145.32 (C-5), 145.23 (C-4), 137.76 (C-2′), 133.05 (C-7), 128.42 (C-4′), 128.22 (C-8), 127.31 (C-6), 121.28 (C-8a), 119.97 (C-5′), 116.66 (C-4a), 44.53 (Cγ), 39.09 (Cα), 30.01 (Cβ). MS-ESI (MeOH) m/z (%): 333 (MH^+, 100). Anal. $C_{14}H_{13}ClN_6O_2 \cdot 0.5$AcOEt (C, H, N).

2.1.4. Synthesis of **3** and **4** (method B)

A solution of 1,4-dichloro-5-nitrophthalazine (0.733 g, 3.0 mmol), 2-(1*H*-imidazol-4-yl)ethanamine (0.666 g, 6.0 mmol), and triethylamine (1.5 mL) in toluene (35 mL) was heated at 100 °C for 5 h. After cooling to room temperature, the solvent was removed under reduced pressure. The residue was purified by flash column chromatography (toluene/ethyl acetate/ethanol, v/v: 0.5/1/0.5). The appropriate fractions (monitored by TLC with the same eluent mixture composition) were combined to give three alkylamination products. The fraction with R_f = 0.27 was discarded as an hydroxilated subproduct. The fraction with R_f = 0.51 afforded 86 mg (9% yield) of a yellow solid, which was identified as 1-[2-(imidazol-4-yl)ethylamino]-4-chloro-8-nitrophthalazine (**3**), mp 133–134 °C. IR (KBr) ν_{max}: 3405, 2925, 1723, 1562, 1214 cm^{-1}. ^{1}H NMR (DMSO-d_6) δ: 8.49 (d, 1H, J = 8.3 Hz, H-7), 8.43 (d, 1H, J = 7.8 Hz, H-5), 8.16 (t, 1H, J = 8.2 Hz, H-6), 7.63 (s, 1H, H-2′), 6.90 (s, 1H, H-5′), 6.79 (brs, 1H, NH-C1), 3.71 (m, 2H, Hα), 2.85 (t, 2H, J = 7.0 Hz, Hβ). ^{13}C NMR (DMSO-d_6) δ: 151.02 (C-1), 145.98 (C-8), 144.27 (C-4), 135.08 (C-2′), 135.00 (C-4′), 133.41(C-6), 129.87 (C-5), 128.83 (C-7), 127.14 (C-4a), 116.39 (C-5′), 110.98 (C-8a), 42.68 (Cα), 25.96 (Cβ). MS-ESI (MeOH) m/z (%): 319 (MH^+, 100). Anal. $C_{13}H_{11}ClN_6O_2 \cdot 0.5H_2O$ (C, H, N). The fraction with R_f = 0.16 afforded 241 mg (25% yield) of a yellow solid, which was identified as 1-[2-(imidazol-4-yl)ethylamino]-4-chloro-5-nitrophthalazine (**4**), mp > 322 °C (dec). IR (KBr) ν_{max}: 3252, 2925, 2854, 1544, 1460, 1413 cm^{-1}. ^{1}H NMR (DMSO-d_6) δ: 8.60 (d, 1H, J = 8.1 Hz, H-6), 8.41 (d, 1H, J = 7.5 Hz, H-8), 8.21 (t, 1H, J = 5.1 Hz, NH-C1), 8.16 (t, 1H, J = 8.1 Hz, H-7), 7.57 (s, 1H, H-2′), 6.87 (s, 1H, H-5′), 3.80 (m, 2H, Hα), 2.96 (t, 2H, J = 7.2 Hz, Hβ). ^{13}C-RMN (DMSO-d_6) δ: 153.61 (C-1), 145.33 (C-4, C-5), 137.59 (C-4′), 135.18 (C-2′), 133.10 (C-7), 129.94 (C-5′), 128.19 (C-8), 127.21 (C-6), 121.28 (C-8a), 116.70 (C-4a), 42.07 (Cα), 26.26(Cβ). MS-ESI (MeOH) m/z (%): 319 (MH^+, 100). Anal. $C_{14}H_{13}ClN_6O_2$ (C, H, N).

2.2. Parasite strain and culture

2.2.1. Epimastigote and trypomastigote forms

Epimastigote forms of *T. cruzi* SN3 strain (IRHOD/CO/2008/SN3) isolated from domestic *Rhodnius prolixus* from Guajira (Colombia) [21] were cultivated *in vitro* in trypanosomes liquid (MTL) with 10% inactivated fetal bovine serum and were kept in an air atmosphere at 28 °C, in Roux flasks (Corning, USA) with a surface area of 75 cm^2, according to a previously described methodology [22]. The transformation of epimastigote to metacyclic forms was achieved by metacyclogenesis induced by culturing a 5-day-old culture of epimastigote that was harvested by centrifugation at 7000 *g* for 10 min at 10 °C. The parasites were then incubated for 2 h at 28 °C at a density of 5 × 10^8 cells/mL in TAU medium (190 mM NaCl, 17 mM KCl, 2 mM $MgCl_2$, 2 mM $CaCl_2$, 8 mM phosphate buffer, pH 6.0). Thereafter, the parasites were incubated in a 1:100 dilution (final epimastigote forms concentration: 5 × 10^6 cells/mL) for 96 h at 28 °C in TAU3AAG medium (TAU supplemented with 10 mM L-proline, 50 mM L-sodium glutamate, 2 mM L-sodium aspartate and 10 mM D-glucose) in 25 mL culture flasks with a layer of culture medium that was not more than 1 cm in depth [23].

2.2.2. Cell culture and cytotoxicity tests

Vero cells (EACC number 84113001), originally obtained from monkey kidneys, were grown in RPMI (Gibco) supplemented with 10% inactivated fetal bovine serum in a humidified 95% air/5% CO_2 atmosphere at 37 °C for 2 days. The cytotoxicity test for Vero cells was performed according to a previously described methodology [22]. After 72 h of treatment, the cell viability was determined by flow cytometry. Thus, 100 μL per well of propidium iodide solution (100 mg/mL) was added and incubated for 10 min at 28 °C in darkness. Afterward, 100 μL per well of fluorescein diacetate (100 ng/mL) was added and incubated under the same conditions. Finally, the cells were recovered by centrifugation at 400 *g* for 10 min and the precipitate was washed with phosphate-buffered saline (PBS). Flow cytometric analysis was performed with a FACSVantage flow cytometer (Becton Dickinson). The percentage viability was calculated in comparison with the control culture. The IC_{50} was calculated using linear regression analysis from the K_c values of the concentrations employed (0.1–100 μM).

2.3. In vitro activity assays

2.3.1. Epimastigote assays (extracellular forms)

The obtained compounds and the reference drug (BZN) were dissolved in DMSO (Panreac, Barcelona, Spain) at a concentration of 0.01% (v/v) and assayed as nontoxic and without inhibitory effects on parasite growth, according to a reported procedure [22]. The compounds were added to the culture medium at dosages of 100, 50, 25, 10, l, 0.5, 0.25, and 0.1 μM. The effects of each compound against epimastigote forms of *T. cruzi* were tested at 72 h using a Neubauer hemocytometric chamber. The antitrypanosomatid effect is expressed as the IC_{50}, that is, the concentration required to give 50% growth inhibition, calculated by linear regression analysis from the K_c values of the concentrations employed.

2.3.2. Amastigote assays (intracellular forms)

Vero cells were grown as described above in RPMI medium (Gibco). Cells were seeded at a density of 1 × 10^4 cells per well in 24-well microplates (Nunc) with rounded coverslips on the bottom and cultured for 2 days. Afterward, the cells were infected *in vitro* with metacyclic forms at a ratio of 10:1 over 12 h. The non-phagocytosed parasites were removed by washing, and then the drugs (at 100, 50, 25, 10, 1, 0.5, 0.25, and 0.1 μM) were added. Vero cells with the drugs were incubated for 72 h at 37 °C in 5% CO_2. The drug activity was determined on the basis of the number of amastigote forms in the treated and untreated cultures in methanol-fixed and Giemsa-stained preparations. The number of amastigote forms was determined by analyzing 200 host cells distributed in randomly chosen microscopic fields. The anti-trypanosomatid effect is expressed as the IC_{50}.

2.4. SOD inhibition studies

Epimastigote *T. cruzi*, cultured as described above, were collected by centrifugation. The pellet was suspended in 3 mL of STE buffer (0.25 M sucrose, 25 mM Tris–HCl, 1 M EDTA, pH 7.8) and the cells were disintegrated through three cycles of ultrasonication, each for 30 s at 60 W. The homogenate was centrifuged for 5 min at 1500 *g* and 4 °C, and the pellet was washed three times in ice-cold STE buffer. This fraction was centrifuged (2500 *g* for 10 min at 4 °C) and the supernatant was collected. The protein concentrations in the supernatant were determined using the Bradford method [24]. The Fe–SOD and CuZn–SOD activities were determined using the method described by Beyer and Fridovich [25], which measures the reduction of nitrobluetetrazolium (NBT) by superoxide ions. Into each cuvette, 845 μL of the stock solution [3 mL of L-methionine

(300 mg, 10 mL^{-1}), 2 mL of NBT (1.41 mg, 10 mL^{-1}) and 1.5 mL of Triton X-100 1% (v/v)] was added, together with 30 μL of the parasite homogenate fraction, 10 μL of riboflavin (0.44 mg, 10 mL^{-1}) and an equivalent volume of the of the compound solution. Five different concentrations were used for each compound (1–100 μM). In the control experiment, the volume was made up to 1000 μL with 50 mM potassium phosphate buffer (pH 7.8), whereas 30 μL of the parasite homogenate fraction was added to mixtures containing the compounds. Then, the absorbance (A_0) was measured at 560 nm in a spectrophotometer. Every cuvette was illuminated with a fixed lamp light for 10 min under constant stirring and the absorbance (A_1) was measured. CuZn–SOD (isolated from human erythrocites), coenzymes, and substrates used in these assays are commercial products and were purchased from Sigma Chemical Co. The obtained data were analyzed using the Newman–Keuls test [25].

2.5. Molecular modeling

Molecular-modeling studies were carried out using the AMBER method implemented in Hyperchem 8.0 package [26], modified by the inclusion of appropriate parameters [27]. Starting structures for compounds **1**–**4** were built by using Hyperchem capabilities. Its geometry was minimized to a maximum energy gradient of 0.1 kcal/mol with the AMBER force field, using the Polak–Ribiere (conjugate gradient) minimizer, and the simulated annealing procedure was used to cover all conformational space. The most stable extended geometry was always used in all calculations of the interaction with the enzyme. To mimic the conditions used in the activity measurements, that is, water as the solvent, all calculations were carried out *in vacuo* with a distance-dependent dielectric constant value [28]. Charge assignations for all atoms was done by means of *ab initio* calculations using the STO-3G basis set, as it is compatible with the AMBER force field, prior to energy minimization using AMBER. The *T. cruzi* Fe–SOD enzyme structure was obtained from the Brookhaven protein data bank (2gpc) and its energy minimized in the same way. Interaction studies were performed, starting from structures with the compound positioned in the border of the enzyme cavity. Entering the cavity was forced using a restraint for the N–Fe distance, slowly decreasing this distance and letting the complex achieve the minimum energy conformation with no restraints, for all the small driving steps, using the same conditions mentioned above.

2.6. Ultrastructural alterations

Epimastigote forms of *T. cruzi* were cultured at a density of 5×10^5 cells/mL in each corresponding medium containing the compounds tested at their IC_{25} concentrations. After 72 h, these cultures were centrifuged at 400 *g* for 10 min and the pellets produced were washed in PBS and then mixed with 2% (v/v) paraformaldehyde/glutaraldehyde in 0.05 M cacodylate buffer (pH 7.4) for 4 h at 4 °C. Following this, the pellets were prepared for TEM study using a previously described technique [29].

2.7. Infection assays

Vero cells were grown under the same conditions expressed over 2 days. Afterward, the cells were infected *in vitro* with metacyclic forms of *T. cruzi* at a ratio of 10:1. The drugs (IC_{25} concentrations) were added immediately after infection and were incubated for 12 h at 37 °C in 5% CO_2. The nonphagocytosed parasites and the drugs were removed by washing, and then the infected cultures were grown for 10 days in fresh medium. Fresh culture medium was added every 48 h. The drug activity was determined from the percentage of infected cells, the number of amastigote forms per infected cell, and the number of trypomastigote forms in the medium [15], in treated and untreated cultures, as well as in methanol-fixed and Giemsa-stained preparations. The percentage of infected cells and the mean number of amastigote forms per infected cell were determined by analyzing 200 host cells distributed in randomly chosen microscopic fields every 48 h. The number of trypomastigote forms in the medium was determined using a Neubauer hemocytometric chamber every 48 h.

2.8. In vivo trypanocidal activity assays

2.8.1. Mice infection and treatment

This experiment was performed using the rules and principles of the international guide for biomedical research in experimental animals and with the approval of the ethical committee of the University of Granada, Spain. Groups of six Balb/c female albino mice (6–8 weeks old, 25–30 g weight) maintained under a 12 h dark/light cycle (lights on at 07:30 h) at a temperature of 22 ± 3 °C and provided with water and standard chow *ad libitum*, were inoculated through the intraperitoneal route with 5×10^3 blood trypomastigote forms of *T. cruzi* per mouse obtained from previously infected mice blood. The animals were divided as follows: **I** positive control group (mice infected but not treated) and **II** study group (mice infected and treated with the compounds under study). The administration of the tested compounds was initiated on the fifth day of infestation once the infection was confirmed, and doses of 25 mg/kg body weight were administered every two days until day 13 pi through the intraperitoneal route. Peripheral blood was obtained from the mandibular vein of each mouse (5 μL samples) and dissolved in 495 μL of PBS solution at a 1:100 dilution. The circulating parasite numbers were quantified with a Neubauer's chamber for counting blood cells. This counting was performed every 3 days over 40 days (acute phase). The number of bloodstream forms was expressed as parasites/mL.

2.8.2. Cyclophosphamide-induced immunosuppression and assessment of the cure

After day 60, the mice entered the chronic phase of the experiment where parasitemia continued decreasing its levels progressively, independently of the treatment. So, on day 150, the parasitemia was checked and found to be undetectable by fresh blood microscopic examination; then, the mice received four intraperitoneal doses of 200 mg/kg w of body mass cyclophosphamide monohydrate (CP) (ISOPAC®) on alternate days, as previously described [30]. The efficacy of such an immunosuppression procedure to assess cryptic infection was verified by the high parasitemias under microscopic examination and/or mortality close to the 100% of chronically untreated mice, having received the immunosuppression treatment. Within 1 week after the last CP injection, parasitemia was evaluated according to the procedure described for the acute phase to quantify the presence of blood trypomastigote forms as a reactivation rate. Finally, the mice were bled out under gaseous anesthesia (CO_2) through a heart puncture and the blood was collected. Blood was incubated for 2 h at 37 °C and then over night at 4 °C in order to allow clotting and to obtain the serum from the samples after centrifuging the supernatant twice at 1000 and 2700 *g*, consecutively. The serum was divided into aliquots and used for ELISA and biochemical analyses, as explained below. Hearts were harvested and immediately flushed free of blood by gentle infusion of 10 mL of prewarmed PBS through the left ventricle [31] in order to avoid contamination of collected tissue with blood parasites. Afterward,

they were frozen at −80 °C and stored until they were used for DNA extraction.

2.9. ELISA tests

Fe−SOD excreted from the parasite, cultured, and processed, as described by Lopez-Céspedes et al. [32], was used as the antigen fraction. The partially purified protein fraction was coated onto polystyrene microtiter plates (Nunc, Denmark) as 1.5 μg in carbonate buffer (pH 8.2) for 2 h at 37 °C. The antigen remaining on the plate was eliminated by washing three times with 0.05% PBS-Tween 20 (washing buffer). Free adsorption sites were taken by incubation (2 h at 37 °C) with blocking buffer [0.2% PBS-Tween 20, 1% bovine serum albumin (BSA)]. After the mixture was washed, as described previously, the plates were incubated (45 min at 37 °C) with a serum dilution of 1:80 in washing buffer. After the second wash, the plates were incubated in darkness for 20 min with 100 μL of an enzyme-conjugated antibody (anti-IgG peroxidase) at a dilution of 1:1000. The enzyme reaction was developed with the chromogenic substrate *o*-phenylenediamine dihydrochloride (OPD, Sigma) and 10 μL of 30% H_2O_2 per 25 mL for 20 min in the dark. The reaction was stopped by the addition of 50 μL of HCl (3 M). The absorbance was read at 492 nm in a microplate reader (Sunrise, TECAN). All of the samples were analyzed in triplicate in polystyrene microtiter plates. Mean and standard deviations of the optical densities of the negative control sera were used to calculate the cutoff value.

2.10. DNA extraction and qualitative PCR

Hearts were thawed and then grinded using a Potter-Elvehjem to follow the purification procedure using a Wizard® Genomic DNA Purification Kit (Promega). PCR was performed with two primers designed in our laboratory [33], based on the published sequence of the enzyme SOD *T. cruzi* CL Brenner (GenBank accession No. XM_808937), which amplifies a fragment of approximately 300 bp, which belong to the SOD gene b of *T. cruzi*. PCR was performed in a total volume of 20 μL. The reaction mixture included 1 μL of DMSO, 200 nM of iSODd, 200 nM of iSODr, 10 mM Tris−HCl (pH 9.0), 1.5 mM $MgCl_2$, 50 mM KCl, 0.01% gelatin, 0.1% triton X-100, 100 mM of each dNTP, 0.5 U of Taq DNA polymerase, 0.5−1 μg of DNA and HPLC water to a final volume of 20 μL. The amplification was performed in a Thermal Cycler TM MyCycler (BioRad) with the following routine temperature: 95 °C/3 min, 30 cycles of 95 °C/30 s, 55.5 °C/45 s, 72 °C/30 s, and 72 °C/7 min. Next, the amplification products were subjected to electrophoresis on 1.6% agarose gel containing 1:10,000 of GelRed™ Nucleic Acid Gel Stain, for 90 min at 90 V.

2.11. Toxicity tests through clinical chemistry measurements

A fraction of the obtained serum was sent to the Biochemical Service at the University of Granada, where a series of parameters were measured according to the commercial kits acquired from Cromakit® by BS-200 Chemistry Analyzer (Shenzhen mindray, Biomedical electronics co., Ltd.). With the levels obtained for different populations of sera, biochemical studies in mice uninfected, infected and in the acute phase, or infected in the chronic phase were performed on 15 individuals. And 6 infected individuals were treated with compound 3 on day 120 m pi. ($n = 15$, $n = 6$), we calculated the mean value and standard deviation. Finally, we also calculated the confidence interval for the mean normal populations based on a confidence level of 95% [$100 \times (1 - \alpha) = 100 \times (1.05)$%]. The obtained ranges are shown in Table 3, which allows the comparison and analysis of the sera studied in this work.

3. Results and discussion

3.1. Synthesis and identification

The starting 1,4-dichloro-5-nitrophthalazine material was prepared from 3-nitrophthalic acid, as shown in Scheme 1, by successive treatment with acetic anhydride, an equivalent amount of aqueous hydrazine hydrate in ethylenglycol, and phosphorous oxychloride/*N*,*N*-dimethylaniline. In the last step, conditions related to those previously established by our group for the synthesis of 1,4-dichloro-5-nitrobenzo[*g*]phthalazine [34] were used, and the dichloro derivative was obtained in a 50% yield. Alkylamino-substituted derivatives **1** and **2** were obtained with respective yields of 15 and 21% through nucleophilic substitution of the chlorine atom attached to the C-1 or C-4 positions, respectively, of 1,4-dichloro-5-nitrophthalazine with 3-(imidazol-1-yl)propylamine by heating in toluene at 85 °C for 2 h, using triethylamine as the chlorine acceptor (method A). Two equivalents of the imidazoleamine were used because that reactant partially decomposes under the reaction conditions required for achieving substitution of the chlorine atom. In contrast with previous related reactions from 1,4-dichlorophthalazine, the formation of the bis(alkylamino)-substituted derivatives was not detected, owing to the deactivating effect of the nitro group on the phthalazine system. However, substitution by hydroxy groups gave side products that were discarded. When the same conditions were used for the preparation of **3** and **4** with 2-(1*H*-imidazol-4-yl)ethanamine as the aminoalkylating agent, compound **3** was not obtained; therefore, different reaction conditions were tested. Finally, increasing the reaction time and temperature to 5 h and 100 °C, respectively, (method B) allowed the isolation of both **3** and **4** in respective yields of 9 and 25%. Isolation of **1**–**4** from the crude reaction mixtures was performed by column flash chromatography with a toluene/ethyl acetate/ethanol mixture of increasing polarity.

All of the newly synthesized compounds were unequivocally identified by their analytical, electrospray ionization mass spectra (MS-ESI), IR, ^{1}H NMR, and ^{13}C NMR spectroscopic data, as shown in the Experimental section. Scheme 1 displays the molecular ions obtained from the electrospray mass spectra, which, in all cases, agree with the proposed structures. For an accurate assignment of the signals in the ^{1}H and ^{13}C NMR spectra, which were registered in deuterated dimethylsulfoxide (DMSO-d_6), heteronuclear simple quantum coherence (gHSQC) and heteronuclear multiple bond coherence (gHMBC) experiments were performed. Registering those bidimensional spectra was very useful, since it allowed us to identify the ^{13}C chemical shifts of every carbon atom, which was crucial for differentiating between the two isomers of each pair of compounds.

The ^{1}H NMR spectra of all of the alkylamino-substituted products showed signals corresponding to the three aromatic protons of the phthalazine system as the two expected doublets and one triplet, whereas the two protons of the imidazole ring appeared as singlets and the integration lines confirmed that they were, in all cases, monoalkylamino-substituted compounds. However, ^{1}H NMR data did not allow us to assign the position of the nitro group in the obtained pairs of isomers. The only relevant difference was a significant deshielding of the NH signal attached to C-1 in compound **2** with respect to **1** (+1.3 ppm) and **4** with respect to **3** (+1.4 ppm). When comparing the NH shifts with those of compounds IV [14], which are devoid of the nitro group, **2** and **4** exhibited very similar values, suggesting that the nitro substituent could be attached to C-5, that is, far from the alkylamino substituent and unable to interact with the NH group, but this was not conclusive. The search for a NOE effect between the NH substituent and the H-8 atom of compound **4** did not give any clear evidence of intramolecular

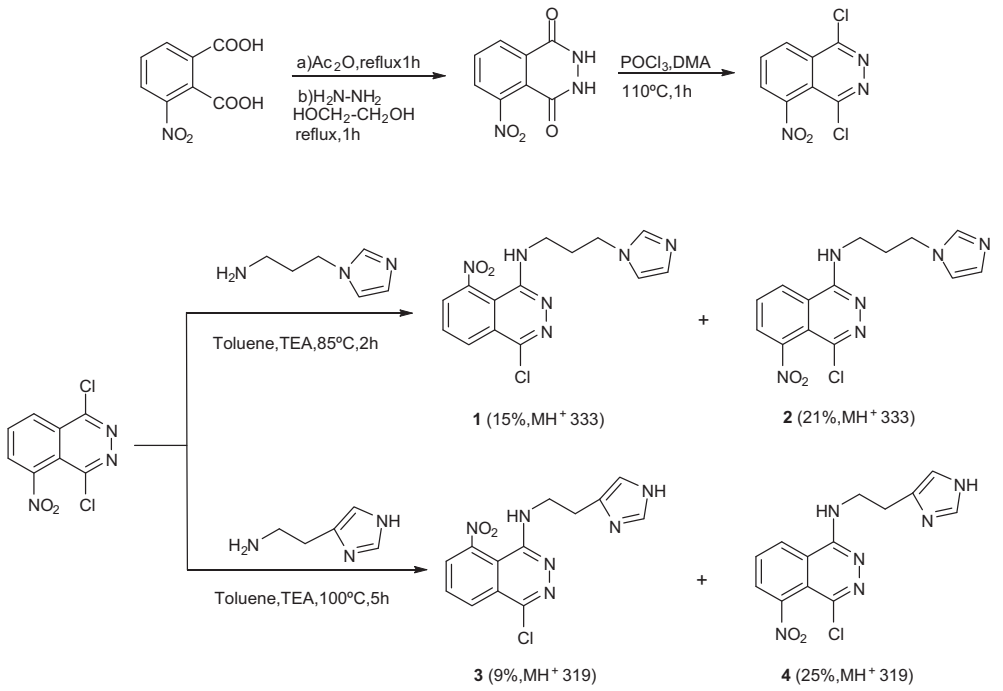

Scheme 1. Preparation of the imidazole-containing nitrophthalazine derivatives **1**–**4**.

interaction. Comparison of the theoretical and experimental ^{13}C spectra of the pairs of isomers was more informative, as remarkable differences were found between the calculated spectra of the phthalazine moiety of the 5-nitro and 8-nitro isomers. As expected, the most significant were those concerning quaternary C-4a and C-8a, located in α and β positions with respect to the carbons supporting the nitro group [35,36]. Table 1 shows the theoretical shift differences found for those carbon atoms between the 5-NO_2 and 8-NO_2 isomers in comparison with the experimental ones, corresponding to the pairs of compounds **1**–**2** and **3**–**4**. It can be seen that the obtained results fit with the assignment proposed previously and that shielding or deshielding of the carbon atoms followed the same pattern in all cases, so that the 5-nitro disposition can be ascribed to compounds **2** and **4**.

3.2. *In vitro* trypanocidal evaluation

In order to obtain preliminary information, the *in vitro* activity of compounds **1**–**4** was evaluated against epimastigote, amastigote, and trypomastigote forms of *T. cruzi* as described in the Experimental section. Epimastigote extracellular forms are the most commonly used, owing to easier handling, but tests performed on intracellular amastigotes are more indicative, as extracellular forms are not the developed form of the parasite in vertebrate hosts [37]. Therefore, Vero cells were infected with metacyclic forms of *T. cruzi*, which were transformed into amastigotes within 1 day of infection and treated with compounds **1**–**4**. Their activity against blood trypomastigotes was also tested, as these forms of the parasite are responsible for the chronic phase of Chagas disease. Table 2 shows the IC_{50} values obtained after 72 h of exposure and at 1–100 μM concentrations when compounds **1**–**4** were assayed against the three parasite forms mentioned above. Values obtained with the reference drug BZN were included in all cases for comparison. It was shown that compound **3** was the most active of the four compounds tested for the three parasite forms assayed, being the best result obtained for intracellular amastigote forms, with an IC_{50} of 4.0 μM, although activity values were homogeneous for the three forms, as they ranged between 4.0 μM and 6.1 μM. Furthermore, compound **3** was more effective than the reference drug in all cases. It is also interesting to note that nitrocompound **3** was more active against amastigote forms than its unsubstituted analog described in Ref. [14] (IC_{50} 4.0 ± 0.3 μM against 9.4 ± 1.2 μM). On the other hand, the cytotoxicity of compounds **1**–**4** was evaluated using mammalian Vero cells as the cellular model (also in Table 2). Interestingly, toxicity data against Vero cells after 72 h of culture showed that all of the assayed phthalazine derivatives were substantially less cytotoxic than BZN, despite the presence of the a priori conflictive nitro group in all of the structures considered. Citotoxicity values ranged from 112.9 to 298.6 μM, which are in sharp contrast to the value obtained for BZN (13.6 μM).

From the *in vitro* data reported above, more informative selectivity index (SI) values could be obtained and are shown in the last columns of Table 2. Good results were found for all of the four compounds in all parasite forms tested when the number of times that the SI of each compound exceeded the SI of BZN (in brackets)

Table 1
Significant differences between the ^{13}C NMR chemical shifts of the phthalazine moiety calculated for the 5-nitro and 8-nitro isomers and those obtained experimentally for the isomer pairs of compounds **1**–**2** and **3**–**4** (measured in ppm).

Carbon	$\Delta\delta_{Theor}$ ($\delta_{8\text{-Nitro}} - \delta_{5\text{-Nitro}}$)	$\Delta\delta_{Exp}$ ($\delta_{Comp\ 1} - \delta_{Comp\ 2}$)	$\Delta\delta_{Exp}$ ($\delta_{Comp\ 3} - \delta_{Comp\ 4}$)
C-4a	+9.3	+10.8	+10.4
C-8a	−9.3	−9.7	−10.9

Table 2
In vitro activity, toxicity, and SI obtained from assays performed with the imidazole-containing phthalazine derivatives **1**–**4** on different forms of *T. cruzi*.

Comp	IC_{50} (μM)[a]			Toxicity IC_{50} Vero cell (μM)	SI[b]		
	Epimastigote forms	Amastigote forms	Trypomastigote forms		Epimastigote forms	Amastigote forms	Trypomastigote forms
Bzn	15.8 ± 1.1	23.3 ± 4.6	22.4 ± 1.9	13.6 ± 0.9	0.8	0.6	0.6
1	10.35 ± 4.9	8.76 ± 1.1	11.0 ± 1.4	152.8 ± 8.3	14.8 (18)	17.4 (29)	13.9 (23)
2	20.6 ± 3.4	17.4 ± 0.9	24.5 ± 4.9	205.7 ± 15.1	10.0 (12)	11.8 (20)	8.4 (14)
3	5.6 ± 0.5	4.0 ± 0.3	6.1 ± 3.5	112.9 ± 8.7	20.2 (25)	28.2 (47)	18.5 (31)
4	22.9 ± 1.8	23.5 ± 2.2	27.1 ± 10.0	298.6 ± 14.3	13.0 (16)	12.7 (21)	11.0 (18)

Values displayed are the mean plus standard deviation derived from four separate determinations.
[a] IC_{50} = concentration that inhibits cell proliferation by 50%. In each case, the IC_{50} was estimated using the regression function with the highest goodness of fit (R^2) at six different concentrations (0.1–100 μM).
[b] Selectivity Index (SI) = IC_{50} Vero cells/IC_{50} *T. cruzi*. In parentheses: number of times that a compound SI exceeds the reference drug SI.

were calculated, with SI values exceeding those of BZN between 12 and 47 times. The best comparative results (29-, 20-, 47-, and 21-fold for compounds **1**, **2**, **3**, and **4**, respectively) were obtained against the most significant intracellular amastigote forms. On the other hand, it was confirmed that the 8-nitrophthalazine derivative (**3**) was the most effective among the compounds tested, as it showed the best SI values against the three forms, being 47 times more selective than BZN when assayed against amastigote forms, whereas the other three compounds exhibited lower and more homogeneous SI numbers, ranging between 20 and 29 times more selective than the reference drug.

3.3. Inhibitory effect on the T. cruzi Fe–SOD enzyme

As mentioned above, the antiparasitic activity of other imidazole-containing pyridazine derivatives was previously related to their inhibitory activity against the Fe–SOD enzyme of the parasite, which could be considered as a potential target for the design of new molecules that are able to act in the iron-moiety environment [13–15]. In order to obtain more evidence, the effects of compounds **1**–**4** on *T. cruzi* Fe–SOD were tested at concentrations ranging from 1 to 100 μM. Epimastigote forms of *T. cruzi* were used, which excrete Fe–SOD when cultured in a medium lacking inactive fetal calf serum (FCS) [38]. The obtained inhibition data are shown in Fig. 3A, and the corresponding IC_{50} values are included in parentheses to make the interpretation of the results easier. For comparison, Fig. 3B shows the effect of the same compounds on commercial CuZn–SOD isolated from human erythrocytes. All four compounds were active against Fe–SOD. However, when looking at Fig. 3A, it can be seen that the most trypanosomicidal compound (**3**) inhibited the enzyme activity to a great extent, whereas the inhibitory activities of compounds **1**, **2**, and **4** were visibly lower. The graph shows that 8-nitro derivative **3** reached 100% inhibition of Fe–SOD at a concentration of 100 μM and inhibited Fe–SOD by more than 60% at 50 μM, whereas the other three compounds stayed below 50% inhibition even at a concentration of 100 μM. Interestingly, the effect of compound **3** on human CuZn–SOD was substantially lower than in the case of Fe–SOD, as the inhibitory activity scarcely reached 30% at a concentration of 100 μM. That selectivity could result in potential activity against Chagas disease with scarce side-effects in human organs. Concerning the IC_{50} data, values higher than 100 μM were obtained in all cases, with the remarkable exception of compound **3**, which gave an IC_{50} of 22 μM against Fe–SOD, being al least five times more inhibitory than the other compounds, whereas an IC_{50} > 100 μM was calculated against CuZn–SOD. Therefore, the highest antipararasitic activity was in correlation with the highest inhibitory activity of Fe–SOD, as found previously for other series of azole-containing phthalazine derivatives.

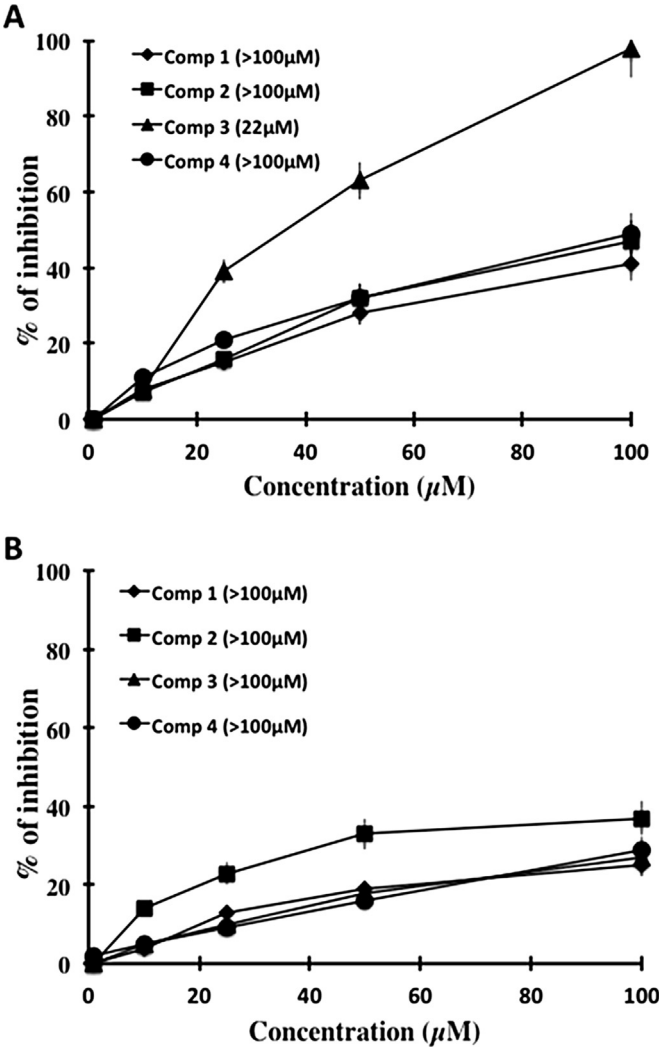

Fig. 3. (A) *In vitro* inhibition (%) of Fe–SOD in *T. cruzi* epimastigotes for compounds **1**–**4** (activity 20.77 ± 3.18 U/mg). (B) *In vitro* inhibition of CuZn–SOD in human erythrocytes for compounds **1**–**4** (activity 23.36 ± 14.21 U/mg). Values are the average of five separate determinations. Differences between the activities of the control homogenate and those incubated with compounds **1**–**4** were obtained according to the Newman–Keuls test. The IC_{50} values were calculated by linear regression analysis from the K_c values at the concentrations used (1, 10, 25, 50, and 100 μM).

3.4. Molecular modeling study

In previous work with related phthalazine derivatives [14,39], we found some correlation between the experimental Fe–SOD

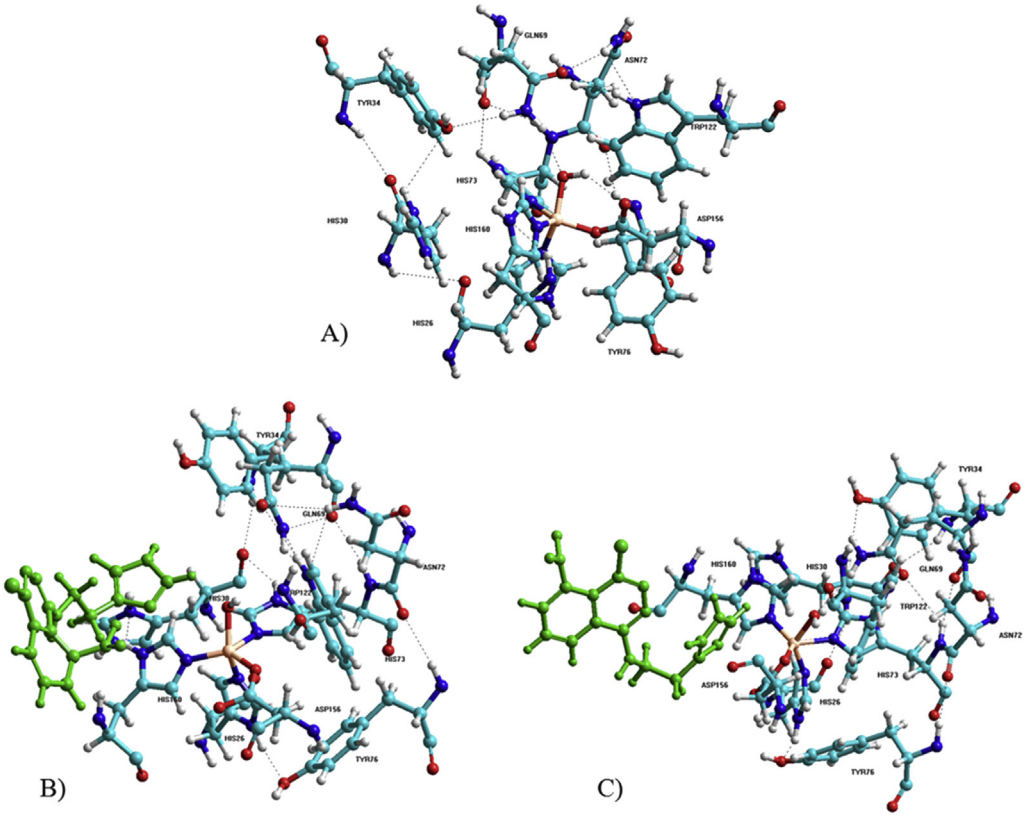

Fig. 4. (A) Molecular model of the free Fe–SOD enzyme active site with its supporting network of hydrogen bonds displayed as dashed lines. (B) and (C) Molecular models of the Fe–SOD enzyme active site with compounds **3** and **4**, respectively, embedded in the proximity of the iron atom, showing the modified H-bonding networks. The inserted nitrophthalazine derivatives are highlighted in green color.

inhibitory activity and theoretical perturbation of the geometry at the enzyme core, both in *T. cruzi* and in *Leishmania* parasites. Therefore, a tentative molecular modeling study on the mode of interaction with the enzyme was performed. The core of an Fe–SOD enzyme monomer contains an iron atom as a five-coordinated active site ligated by three histidine units, an aspartate group, and an axial H_2O or HO^- ligand supported by an essential H-bonding network, comprised of amino acids [40]. Specifically, the coordinated solvent engages in H bonds with the Asp156-ligand and with the conserved active site Gln69 [41] (Fig. 4A). Several studies have emphasized the importance of those ligands and its H-bonding partners in tuning the antioxidant activity of Fe–SOD [42]. The coordinated solvent acts as a proton donor/acceptor, thereby facilitating the release of peroxide generated in the reduction of the substrate [41], and it also plays a critical role in modulating the reduction potential of the iron center [42]. It is supposed that the protonation state is strongly influenced by H bonding with Gln69 and, in turn, H bonds to a network including Tyr34, Asn72, and Trp122, among others. On that basis, it has been proposed that enzyme inhibition could take place by modification of the H-bonding system induced by irruption of an external compound [43].

The ability of related benzo[*g*]phthalazine derivatives to modify the H-bonding network at the active site of the Fe–SOD enzyme (obtained from the Brookhaven protein data bank 2gpc entry) had been tested previously using the Amber force field implemented in Hyperchem 8.0 [14,39]; the methodology used is specified in the Experimental section. Fig. 4A shows the active site of the enzyme, with the H-bonding system outlined above displayed as dashed lines and the solvent ligand in the foreground linked to the iron atom. The key interactions with Gln69 and Asp156 are clearly seen. The highly inhibitory 8-nitrophthalazine derivative **3** was then buried into one monomer with the imidazole ring pointing towards the metal ion, and the energetically most favored disposition was identified (Fig. 4B). As a consequence of the approach of the molecule, the amino acids surrounding the iron atom were displaced, apart from their initial positions and the H-bonding pattern appeared remarkably distorted. The three histidine molecules and Tyr34 were especially affected, but the most relevant point was that the H bonds of the H_2O/HO^- ligand with Gln69 and Asp156 were missing, as both amino acids moved towards the rear of the active center, as seen in the Figure and, consequently, the hydroxyl ligand remained too far away for creating stable interactions with them. In fact, the $H_{Gln}–O_{lig}$ and $O_{Asp}–H_{lig}$ distances increased from 2.30 to 3.61 Å and from 2.32 to 4.57 Å, respectively. In a further step, the same molecular modeling treatment was given to the less inhibitory isomer **4** (Fig. 4C). It was found that the presence of the molecule also disturbed the H-bonding network surrounding the active center, but, interestingly, the hydrogen bond between Gln69 and the H_2O/HO^- ligand was maintained with a calculated $H_{Gln}–O_{lig}$ distance of 2.52 Å, whereas that corresponding to the $O_{Asp}–H_{lig}$ disappeared, as the aspartate oxygen was now located very far from the ligand's hydrogen atom, at a distance of 5.40 Å. We think that these theoretical calculations could explain, in part, the remarkable inhibitory effect found experimentally for compound **3**.

Both the trypanocidal activity and Fe–SOD inhibitory properties explained above supported the convenience of carrying out more detailed *in vitro* and *in vivo* assays with the 8-nitrophthalazine derivative **3** in order to obtain more information about its mode

of action and its apparent advantages with respect to BZN. In accordance with the usual working procedure, compounds **1**, **2**, and **4** were not tested in further studies, owing to the less significant SI results obtained.

3.5. Infectivity assay

To gain better insight into the trypanocidal activity of compound **3**, its effect on the infectivity and intracellular replication of *T. cruzi* amastigotes was subsequently determined. The propagation of the parasite in Vero cells was evaluated by measuring the infection rates and the average number of amastigotes and trypomastigotes present during a 10-day treatment period. Vero cells were cultured for 2 days and then infected with epimastigote forms in the stationary phase. The parasites invaded the cells and underwent morphological conversion to amastigotes within 2 days of infection. The IC_{25} was used as the test dosage and BZN was the reference drug. On day 8, the rate of host-cell infection reached its maximum in the control experiment. When 8-nitrophthalazine derivative **3** was added to the infected Vero cells, a remarkable decrease in host-cell infection rate, which reached 95% on day 8 and remained stationary until day 10, was observed, making compound **3** much more effective than the reference drug, which only afforded a mere 20% reduction on day 10 (Fig. 5A). The measure of the mean number of amastigotes per infected Vero cell (Fig. 5B) led to similar results; at the end of the treatment, the nitrophthalazine derivative had decreased the number of amastigotes present in the cells by 74%, whereas BZN only allowed a poor reduction of 15%. Regarding the number of trypomastigote forms released in the medium (Fig. 5C), the inhibition values were generally less significant. Even so, compound **3** reached 55% reduction and almost doubled the inhibitory effect of BZN (30%), which remained less effective. Ultimately, infectivity tests confirmed the *in vitro* antiparasitic activity shown in Table 2 for compound **3**, as well as its higher efficacy with respect to the reference drug.

3.6. Ultrastructural alterations

The remarkable trypanosomicidal activity shown by 8-nitrophthalazine derivative **3** should cause important damage in the parasite cells. Therefore, the morphological alterations created in *T. cruzi* epimastigotes were analyzed using TEM in order to obtain some information about the way the cell structure was affected. The most significant variations compared to the control cells are shown in Fig. 6 for parasites treated with compound **3**. As expected, highly significant alterations were found. Some parasites died (second panel in Fig. 6) and deep modifications were evident in most of the rest. The shape of many parasites was heavily distorted, as they were very swollen with cytoplasms filled with empty vacuoles and other vacuoles containing large amounts of electron-dense material (third panel in Fig. 6). Some mitochondria were also swollen and devoid of crypts, looking like vacuoles filled with a more dense content than that of lipidic ones. Others were filled with smaller vacuoles, and kinetoplasts were very swollen and disorganized. The number of ribosomes present in treated epimastigotes was much lower than that found in the control cultures (third panel in Fig. 6). These findings, regarding essential modifications in the composition of the parasite cells, are consistent with the significant trypanocidal activity data found for compound **3**.

3.7. In vivo anti-T. cruzi activity in Balb/c female albino mice

As compound **3** showed remarkable SI values with respect to BNZ in the *in vitro* experiments and was the best inhibitor of the parasitic Fe–SOD enzyme, it was selected for further *in vivo* studies

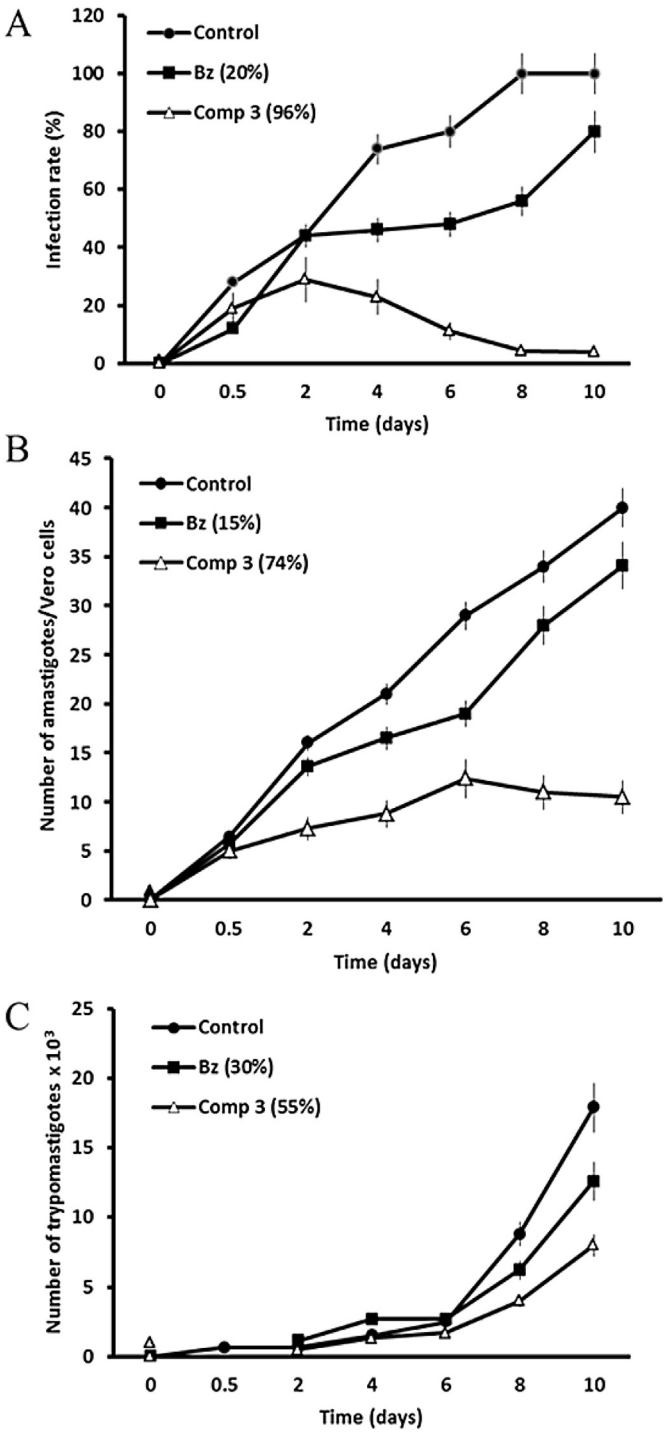

Fig. 5. Effect of compound **3** on the infection rate and growth of *T. cruzi*: (A) rate of infection, (B) mean number of amastigotes per infected Vero cell, and (C) number of trypomastigotes in the culture medium. (▲) control, (■) BZN, (Δ) compound **3**. Measured at IC_{25}. Values are the means of three separate experiments.

in the chosen murine model. The trypanocidal activity during the acute phase of Chagas disease [until 40 days post infection (pi)] was first investigated. Female Balb/c mice were inoculated with 5×10^3 blood trypomastigotes obtained from a mouse previously infected. We opted for the intraperitoneal doping route, which usually leads to lower mortality rates than the intravenous procedure [44], and 125 mg of compound **3**/kg of body mass (mpk) were administered in five doses of 25 mpk every two days from the fifth day of

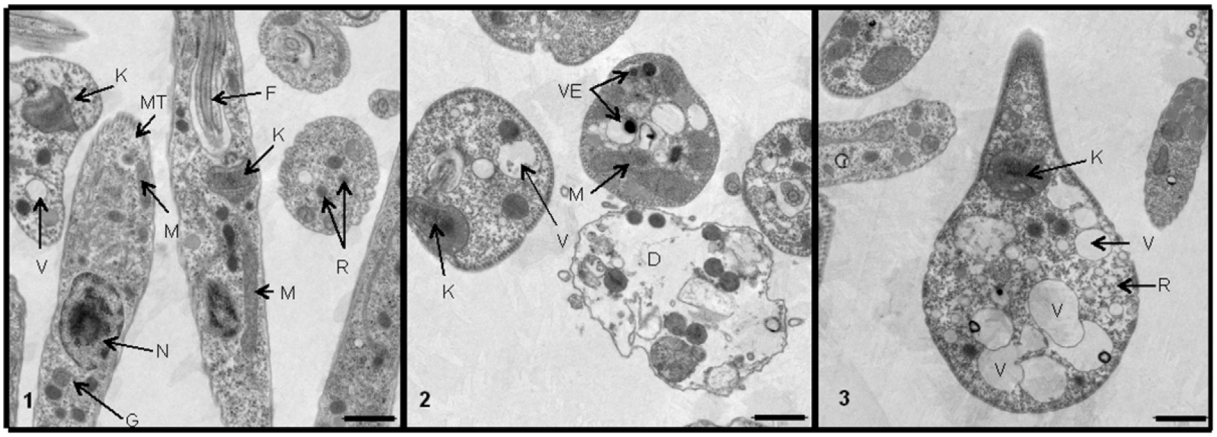

Fig. 6. Ultrastructural alterations found in epimastigote forms of *Trypanosoma cruzi*. **1**: Control of *T. cruzi* untreated parasites with its typical aspect; **2**–**3**: epimastigote forms treated with compound **3**. Key: dead parasite (D), flagellum (F), glycosomes (G), kinetoplast (K), mitochondrion (M), microtubules (MT), nucleus (N), ribosomes (R), vacuoles (V), and vacuoles with electron-dense material (VE). Scale bar = 1 μm.

infestation until day 13 pi, according to the pharmacokinetic of the compound (data not shown). Parasite counting was performed on 5 μL blood samples obtained from the mandibular vein. Interestingly, none of the animals treated with compound **3** died during the treatment, despite the mammalian toxicity typically ascribed to the nitro functional group in antiparasitic drugs. Fig. 7A shows the effect caused by nitrophthalazine derivative **3** on the parasitemia levels in blood during the acute phase of Chagas disease (0–40 days pi). A reduction of parasitemia in mice treated with **3** was evident as early as the beginning of the treatment (day 5 pi), and was maintained, not only until the end of treatment, but to the end of the acute phase. Reduction of parasitemia was not found in mice treated with BZN under the same conditions. The next step was to evaluate the behavior of **3** in the chronic phase, in which the positive effect of the current drugs is under much discussion [45]. From day 120 pi, parasitemia remaining in the blood is virtually undetectable and the parasite is nested inside the target organs in the amastigote form. A major problem during the treatment of Chagas

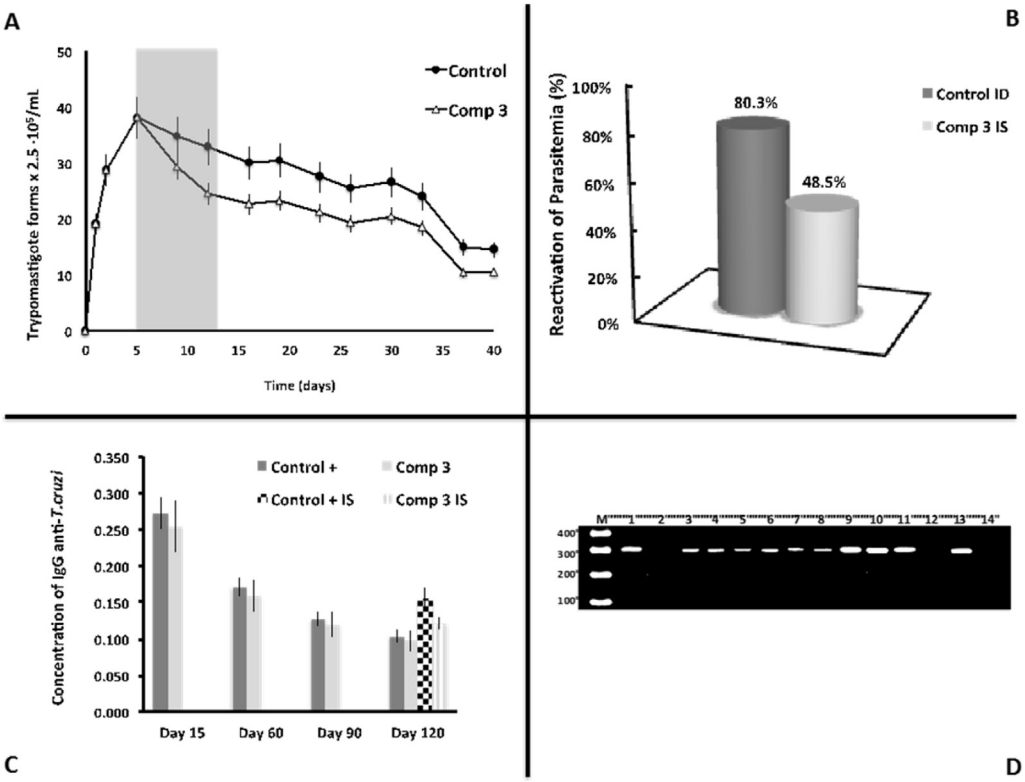

Fig. 7. *In vivo* results obtained for the murine model in Balb/c mice. (A) Activity in the acute phase of Chagas disease: control (-●-) and mice treated with compound **3** (-Δ-), receiving an amount of 125 mg/kg of body mass (grey represents the days of treatment). (B) Reactivation percentage of parasitemia after immunosuppression: the control mice were compared with the non-immunosupressed group treated with compound **3** at the same dosage. (C) Total IgG levels of anti-*T. cruzi*. (D) PCR analysis of heart tissue from different mice groups after necropsy. M: marker; **1**: PCR positive control; **2**: PCR negative control; **3**–**8**: infection control group; **9**–**14**: infected and **3**-treated group. For (A) and (C), values are the means of three separate experiments and error bars represent the mean ± standard deviation.

Table 3
Appraisal of histopathological alterations found in the heart of mice infected with *T. cruzi*: Untreated and treated with compound 3 (120 mg/kg of body mass) after 120 dpi.

Histopathological changes	Control + (untreated)	Treated with comp. 3
Epicardium structure	Normal	Normal
Myocardial structure	Normal	Normal
Endocardium structure	Normal	Normal
Inflammatory infiltrates in the myocardium	+++	+
Subepicardial fibrosis	+++++	+
Cardiomyocyte degeneration	++++	++
Coronary stenosis	No	No

Keys for damage level: + mild; ++ light; +++ moderate; ++++ abundant; +++++ severe.

disease is the high reactivation ability of the parasitemia in immunocompromised individuals cured with apparent success. It has been shown that apparently cured patients who had been submitted to kidney or liver transplantation, diagnosed with AIDS, or treated with anticancer chemotherapy, experimented Chagas reactivation with a very aggressive clinical course [46]. In order to obtain information about this matter, the mice treated as described above were kept until day 120 pi and were subsequently divided into two subgroups, one of which was maintained under the same conditions without further treatment, whereas the other was subjected to three successive cycles of immunosuppression with cyclophosphamide monohydrate, as described in the Material and methods Section [47]. That treatment caused the reactivation of parasitemia, which was controlled previously by the immune system of the mouse. Blood samples were extracted to determine the parasitemia levels of treated mice in comparison with the corresponding non-immunosuppressed subgroup of mice. As reactivation is proportional to the survival rate of the parasites, the effect caused by compound **3** could be estimated and is depicted in Fig. 7B in the form of an illustrative tridimensional graph. Parasitemia reactivation reached 80.3% with respect to the acute phase in the control group of infected and untreated mice, whereas it decreased to 48.5% in the treated mice group, revealing a significant effect on the chronic course of infection. The result was confirmed by evaluating the immunological status of mice involved in the experiment. The detection of total immunoglobuline G (IgG) allows evaluation of the immune status of the mice, as IgG indicates the level of protection that should be attributed to the tested compounds, as well as the innate protection that mice have naturally. According to the previous reports, IgG titres in Balb/c become stable during the chronic phase of the disease [48]. The enzyme-linked immunosorbent assay (ELISA) was used to detect the IgG levels [34], and the antigen source was the Fe−SOD enzyme isolated in our laboratory. The control IgG levels followed the expected pattern for nonspecific hypergammaglobulinaemia at the beginning of infection and remained stable when the infection became chronic. After the immunosuppression treatment, parasitemia reactivation induced a response with increased levels of specific IgG isotypes. Fig. 7C shows that reactivation is lower in mice treated with compound **3** than in untreated mice, confirming the ability of **3** to reduce parasitemia. However, reactivation had found to be better in its unsubstituted analog [14], maybe due to the different pharmacokinetic properties of both molecules. Lastly, Fig. 7D represents the results obtained from a qualitative polymerase chain reaction (PCR) assay [49] performed after necropsy for the evaluation of the parasitic load in cardiac tissue of mice in both the control and treated groups. The hearts were ground and used for total DNA extraction and amplification of a fragment of 278 bp, belonging to SOD gene b of *T. cruzi*. The hearts of control animals confirmed the presence of parasites, whereas those of mice treated with **3** (lanes 9–14 in Fig. 7D) were free of parasites in two of the six cases studied, indicating a 33% percentage of curing. Therefore, the PCR assay also indicated partial effectivity of compound **3** at the administered dose.

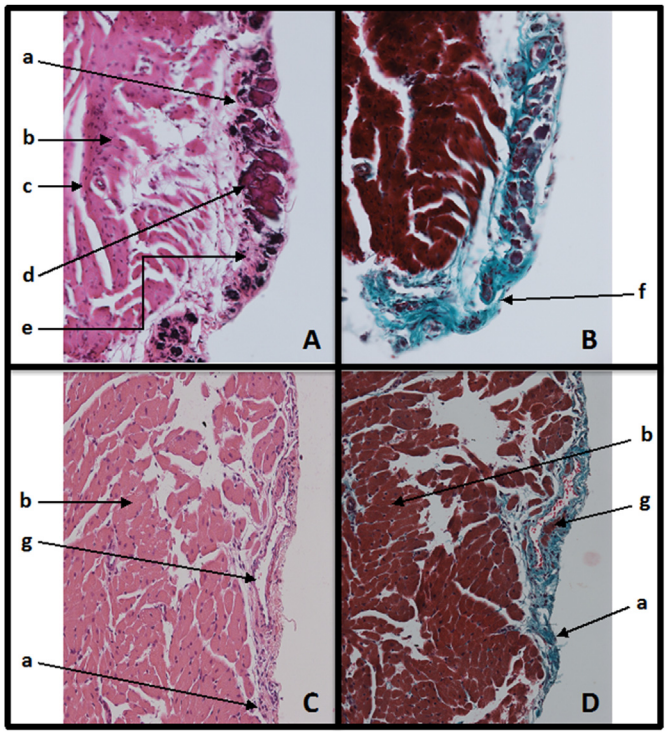

Fig. 8. Histopathological analysis of the hearts after necropsy (120 dpi) at 200 × magnification. (A) Untreated infected mice stained with H&E; (B) untreated infected mice stained with Trichrome; (C) infected and compound-**3**-treated mice stained with H&E; (D) infected and **3**-treated mice stained with Trichrome. Key: **a**: epicardium; **b**: myocardium; **c**: cardiac vein; **d**: cardiomyocytes; **e**: subepicardium; **f**: subepicardial fibrosis; **g**: epicardial capillary.

3.8. Histopathological alterations

As discussed above, interactions between the parasite and the target organs of the guest generate serious damage at morphological and structural levels. Furthermore, the action of the immune system against the infection may cause huge cell distruction inside the organ, as the parasite is in an intracellular location and its elimination is inextricably linked to obliteration of the related cell. As a consequence, we evaluated the damage caused by the parasite in the heart of infected mice during the chronic phase of the disease in both the control and treated groups. The first column of Table 3 lists the most common traces of histopathological cardiac damage, corresponding to a *T. cruzi* infection. Columns 2 and 3 display the results observed after examination of hearts of untreated mice and **3**-treated mice 120 days pi, respectively. From the comparison of

Table 4
Biochemical clinical parameters studied in Balb/c mice uninfected and infected with *T. cruzi* in different experimental situations.

Tested mice groups	Kidney markers		Heart markers		Liver markers			
	Urea (mg/dL)	Uric acid (mg/dL)	CK-MB (U/L)	LDH (U/L)	AST/GOT (U/L)	ALT/GPT (U/L)	Total bilirubin (mg/dL)	Phosphate alkaline (U/L)
Uninfected (n = 15)	39 [36–43]	5 [4.3–5.5]	453 [215–690]	3086 [2108–4064]	126 [103–148]	46 [37–54]	0.23 [0.17–0.28]	133 [104–161]
Infected acute phase (n = 15)	49 [39–60]	4.5 [3.7–5.5]	681 [400–950]	2910 [1589–4232]	129 [100–157]	48 [38–58]	0.15 [0.12–0.18]	231 [161–300]
Infected chronic phase (n = 15)	49 [40–60]	4.3 [3.5–5.0]	800 [500–990]	2536 [1560–4123]	148 [119–170]	53 [40–60]	0.12 [0.10–0.16]	186 [156–250]
Treated with 3, day 120 pi (120 mg/kg w) (n = 6)	=	=	++	−	=	=	=	=

Keys (with respect to profiles of mice infected in the chronic phase): =: variation lower than 10%; ++: up to 30% increasing over the range; −: up to 10% decrease over the range.

the data obtained with both groups, it can be seen that treatment with the nitrophthalazine derivative results in a decrease in cardiac damage, as inflammatory infiltrates change from moderate to mild, subepicardial fibrosis is reduced from severe to mild, and degeneration of cardiomyocites declines from abundant to light. This improvement in histopathological heart alterations after the administration of **3** is confirmed by images obtained after necropsy, which are included in Fig. 8. Panels A and B show the condition of the organ in an infected control mouse using two different staining methods. Panels C and D display alterations found in an infected mouse treated with compound **3**. Strong subepicardial fibrosis and cardiomyocite degeneration are observed in panels A and B, whereas panels C and D indicate a situation with scarce or even nonexistent fibrosis symptoms. All of these data confirm the beneficial effect of the administration of compound **3** on the infected organ during the chronic stage of the disease.

3.9. Biochemical parameter alterations

It is known that the presence of the nitro group in molecules with potential anti-*T. cruzi* properties often results in harmful side effects, affecting essential organs of the guest. For that reason, we studied the biochemical kidney, heart, and liver profiles in mice treated with the nitrophthalazine derivative **3** in order to evaluate the toxicity of this compound after its administration and further metabolization. Later, serum samples were collected during necropsy (final day of the experiment) to determine whether some irreversible toxicity or chronic damage could be detected at that stage in the above mentioned organs. Table 4 shows the most significant marker profiles obtained for the three organs in three groups of mice: uninfected, infected and acute phase, or infected in the chronic phase. Significant alterations in the parameters range of the two infected groups are clearly seen with respect to the uninfected mice. The last file displays how the markers profiles in the chronic phase are affected in mice treated with compound **3**. It is shown that there are no relevant changes in either the kidney or liver markers tested and, therefore, those organs are not damaged by the administration of **3**, even at the relatively high dose used in the assays. Concerning heart markers, mild variations in the CK-MB enzyme levels (with an increase lower than 30%) and in the LDH value (with a decrease of about 10%) are indicative that curing was not complete, as deduced from the histopathological heart images of Fig. 8. So it seems that compound **3** does not cause relevant toxicity in the key organs considered at the administered doses.

We conclude that the introduction of nitro groups into alkylaminophthalazine derivatives functionalized with imidazole rings allowed us to obtain a new compound with better *in vitro* selectivity-index values against *T. cruzi* than BZN. That compound also exhibited selective inhibitory ability against the Fe–SOD enzyme and, causing great damage to the parasite cells, does not result in significant alterations in the key organs of mice tested after its administration in the chronic stage of Chagas disease.

Acknowledgments

The authors thank the MCINN Projects Consolider Ingenio CSD2010-00065 and CTQ2009-14288-C04-01 for financial support. We are also grateful to the NMR and Elemental Analysis C.A.I.s of the Universidad Complutense (Madrid), and also to the transmission electron microscopy and nuclear magnetic resonance spectroscopy services of the CIC-University of Granada. F.O. is grateful for a FPU grant from the Ministry of Education of Spain.

Appendix A. Supplementary data

Supplementary data related to this article can be found at http://dx.doi.org/10.1016/j.ejmech.2015.10.034.

References

[1] (a) A. Cavalli, M.L. Bolognesi, Neglected tropical diseases: multi-target-directed ligands in the search for novel lead candidates against Trypanosoma and Leishmania, J. Med. Chem. 52 (2009) 7339–7359;
(b) S. Espuelas, D. Plano, P. Nguewa, M. Font, J.A. Palop, J.M. Irache, C. Sanmartín, Innovative lead compounds and formulation strategies as newer kinetoplastid therapies, Curr. Med. Chem. 19 (2012) 4259–4288.
[2] WHO, Chagas Disease: Fact Sheet N° 349, March 2014. http://www.who.int/mediacentre/factsheets/fs340/en/.
[3] A. Rassi Jr., A. Rassi, J.A. Marin Nieto, Chagas disease, Lancet 375 (2010) 1388–1402.
[4] J.A. Urbina, Specific chemotherapy of Chagas disease: relevance, current limitations and new approaches, Acta Trop. 115 (2010) 55–68.
[5] J.C. Dujardin, D. González-Pacanowska, S.L. Croft, O.F. Olesen, G.F. Späth, Collaborative actions in anti-trypanosomatid chemotherapy with partners from disease endemic areas, Trends Parasitol. 26 (2010) 395–403.
[6] P.M.M. Guedes, G.K. Silva, F.R.S. Gutierrez, J.S. Silva, Current status of Chagas disease chemotherapy, Expert Rev. Anti Infect. Ther. 9 (2011) 609–620.
[7] R. Viotti, C. Vigliano, B. Lococo, M.G. Alvarez, M. Petti, G. Bertocchi, A. Armenti, Side effects of Bnz as treatment in chronic Chagas disease: fears and realities, Expert Rev. Anti Infect. Ther. 7 (2009) 157–163.
[8] (a) C.J. Schofield, J. Jannin, R. Salvatella, The future of Chagas disease control, Trends Parasitol. 22 (2006) 583–588;
(b) J.D. Maya, D.K. Cassels, P. Iturriaga-Vasquez, Mode of action of natural and synthetic drugs against *Trypanosoma cruzi* and their interaction with the mammalian host, Comp. Biochem. Phys. A 146 (2007) 601–620.
[9] S.R. Wilkinson, C. Bot, J.M. Kelly, B.S. Hall, Trypanocidal activity of nitroaromatic prodrugs: current treatments and future perspectives, Curr. Top. Med. Chem. 11 (2011) 2072–2084.
[10] M.N. Soeiro, S.L. de Castro, *Trypanosoma cruzi* targets for new chemotherapeutic approaches, Expert Opin. Ther. Targets 13 (1) (2009) 105–121.
[11] A.F. Miller, Superoxide dismutases: active sites that save, but a protein that kills, Curr. Opin. Chem. Biol. 8 (2004) 162–168.
[12] J.F. Turrens, Oxidative stress and antioxidant defences: a target for the treatment of diseases caused by parasitic protozoa, Mol. Aspects Med. 25 (2004) 211–220.
[13] A.M. Sanz, F. Gómez-Contreras, P. Navarro, M. Sánchez-Moreno, S. Boutaleb-Charki, J. Campuzano, M. Pardo, A. Osuna, C. Cano, M.J.R. Yunta, L. Campayo, Efficient inhibition of Fe-SOD and of *Trypanosoma cruzi* growth by benzo[g] phthalazine derivatives functionalized with one or two imidazole rings, J. Med. Chem. 51 (2008) 1962–1966.
[14] M. Sánchez-Moreno, F. Gómez-Contreras, P. Navarro, C. Marín, F. Olmo, M.J.R. Yunta, A.M. Sanz, M.J. Rosales, C. Cano, L. Campayo, Phthalazine

derivatives containing imidazole rings behave as Fe-SOD inhibitors and show remarkable anti-*T. cruzi* activity in immunodeficient-mouse mode of infection, J. Med. Chem. 55 (2012) 9900–9913.
[15] M. Sánchez-Moreno, A.M. Sanz, F. Gómez-Contreras, P. Navarro, C. Marín, I. Ramírez-Macias, M.J. Rosales, F. Olmo, I. García-Aranda, L. Campayo, C. Cano, F. Arrebola, M.J.R. Yunta, *In vivo* trypanosomicidal activity of imidazole- or pyrazole-based benzo[g]phthalazine derivatives against acute and chronic phases of Chagas disease, J. Med. Chem. 54 (2011) 970–979.
[16] S. Patterson, S. Wyllie, Nitro drugs for the treatment of trypanosomatid diseases: past, present, and future prospects, Trends Parasitol. 30 (2014) 289–298.
[17] R.B. Oliveira, A.P. Passos, R.O. Alves, A.J. Romanha, M.A.F. Prado, J.D. de Souza Jr., R.J. Alves, *In vitro* evaluation of the activity of aromatic nitrocompounds against, Trypanosoma cruzi, Mem. Inst. Oswaldo Cruz 98 (1) (2003) 141–144.
[18] (a) M.V. Papadopoulou, W.D. Bloomer, H.S. Rosenzweig, S.R. Wilkinson, M. Kaiser, Novel nitro(triazole/imidazole)-based heteroarylamides/sulfonamides as potential antitrypanosomal agents, Eur. J. Med. Chem. 87 (2014) 79–88;
(b) M.V. Papadopoulou, W.D. Bloomer, G.I. Lepesheva, H.S. Rosenzweig, M. Kaiser, B. Aguilera-Venegas, S.R. Wilkinson, E. Chatelain, J.R. Ioset, Novel 3-nitrotriazole-based amides and carbinols as bifunctional antichagasic agents, J. Med. Chem. 58 (2015) 1307–1319;
(c) B. Muro, F. Reviriego, P. Navarro, C. Marín, I. Ramírez-Macías, M.J. Rosales, M. Sánchez-Moreno, V.J. Arán, New perspectives on the synthesis and antichagasic activity of 3-alkoxy-1-alkyl-5-nitroindazoles, Eur. J. Med. Chem. 74 (2014) 124–134.
[19] D.D. Perrin, W.L.F. Armarego, D.R. Perrin, Purification of Laboratory Chemicals, Pergamon Press, Oxford, 1980.
[20] H.D.K. Drew, R.F. Garwood, Chemiluminiscent organic compounds. Part VII. Substituted phthalazine-1,4-diones. effect of the substituent on the luminescent power, J. Chem. Soc. (1939) 836–838.
[21] J. Téllez-Meneses, A.M. Mejía-Jaramillo, O. Triana-Chávez, Biological characterization of *Trypanosoma cruzi* stocks from domestic and sylvatic vectors in Sierra Nevada of Santa Marta, Colombia, Acta Trop. 108 (2008) 26–34.
[22] F. Olmo, C. Marín, M.P. Clares, S. Blasco, M.T. Albelda, C. Soriano, R. Gutiérrez-Sánchez, F. Arrebola-Vargas, E. García-España, M. Sánchez-Moreno, Scorpiand-like azamacrocycles prevent the chronic establishment of *Trypanosoma cruzi* in a murine model, Eur. J. Med. Chem. 70 (2013) 189–198.
[23] J. Cardoso, M.J. Soares, *In vitro* effects of citral on *Trypanosoma cruzi* metacyclogenesis, Mem. Inst. Oswaldo Cruz 5 (2010) 1026–1032.
[24] M.M. Bradford, A refined and sensitive method for the quantification of microgram quantities of protein utilizing the principle of protein-dye binding, Anal. Biochem. 72 (1976) 248–254.
[25] W.F. Beyer, I. Fridovich, Assaying for superoxide dismutase activity: some large consequences of minor changes in conditions, Anal. Biochem. 161 (1987) 559–566.
[26] D.A. Case, T.E. Cheatham, T. Darden, H. Gohlke, R. Luo, K.M. Merz, A. Onufriev, C. Simmerling, B. Wang, R.J. Woods, The amber biomolecular simulation programs, J. Comput. Chem. 26 (2005) 1668–1688.
[27] C. Miranda, F. Escartí, L. Lamarque, M.J.R. Yunta, P. Navarro, E. García-España, M.L. Jimeno, New 1H-pyrazolecontaining polyamine receptors able to complex L-glutamate in water at physiological pH values, J. Am. Chem. Soc. 126 (2004) 823–833.
[28] F. Reviriego, P. Navarro, E. García-España, M.T. Abelda, J.C. Frías, A. Domenech, M.J.R. Yunta, R. Costa, E. Ortí, Diazatetraester 1*H*-pyrazole crowns as fluorescent chemosensors for AMPH, METH, MDMA (ecstasy), and dopamine, Org. Lett. 10 (2008) 5099–5102.
[29] I. Ramírez-Macías, C. Marín, R. Chahboun, I. Messouri, F. Olmo, M.J. Rosales, R. Gutierrez-Sánchez, E. Alvarez-Manzaneda, M. Sánchez-Moreno, *In vitro* and *in vivo* studies of the trypanocidal activity of four terpenoid derivatives against *Trypanosoma cruzi*, Am. J. Trop. Med. Hyg. 87 (2012) 481–488.
[30] S. Cencig, N. Coltel, C. Truyens, Y. Carlier, Parasitic loads in tissues of mice infected with *Trypanosoma cruzi* and treated with AmBisome, PLoS Negl. Trop. Dis. 5 (2011) e1216.
[31] X. Ye, J. Ding, X. Zhou, G. Chen, S.F. Liu, Divergent roles of endotelial NF-kappaB in multiple organ injury and bacterial clearance in mouse models of sepsis, J. Exp. Med. 205 (2008) 1303–1315.
[32] A. Lopez-Céspedes, E. Villagran, K. Briceño-Alvarez, J.A. de Diego, H.L. Hernandez-Montiel, C. Saldaña, M. Sánchez-Moreno, C. Marín, Trypanosoma cruzi: seroprevalence detection in suburban population of Santiago de Queretaro (Mexico), Sci. World J. (2012) 6, http://dx.doi.org/10.1100/2012/914129. Article ID 363595.
[33] F. Olmo, J. Escobedo-Ortega, P. Palma, M. Sánchez-Moreno, A. Mejía-Jaramillo, O. Triana, C. Marín, Specific primers design based on the superoxide dismutase b gene for *Trypanosoma cruzi* as a screening tool: validation method using strains from Colombia classified according to their discrete typing unit, Asian Pac. J. Trop. Med. 7 (11) (2014) 854–859.
[34] L. Campayo, B. Jiménez, T. Manzano, P. Navarro, Diazapolycyclic compounds XXV. Improved synthesis of 6-substituted 2,3-dihydrobenzo[g]phthalazine-1,4-dione derivatives, Synthesis (1985) 197–200.
[35] F. Reviriego, P. Navarro, A. Domenech, E. García-España, Effective complexation of psychotropic phenethylammonium salts from a disodium dipyrazolate salt of macrocyclic structure, J. Chem. Soc. Perkin Trans. 2 (2002) 1634–1638.
[36] V.J. Arán, M. Kumar, J. Molina, L. Lamarque, P. Navarro, E. García-España, J.A. Ramírez, S.V. Luis, B. Escudero, Synthesis and protonation behavior of 26-membered oxaaza and polyaza macrocycles containing two heteroaromatic units of 3,5-disubstituted pyrazole or 1-benzylpyrazole. A potentiometric and ^{1}H and ^{13}C NMR study, J. Org. Chem. 64 (17) (1999) 6135–6146.
[37] A. González-Coloma, M. Sánchez-Moreno, *In vitro* activity of C20-diterpenoid alkaloid derivatives in promastigotes and intracellular amastigotes of *Leishmania infantum*, Int. J. Antimicrob. Agents 25 (2005) 136–141.
[38] M.E. Villagran, C. Marín, I. Rodríguez-González, J.A. de Diego, M. Sánchez-Moreno, Use of an iron superoxide dismutase excreted by *T. cruzi* in the diagnosis of Chagas disease: seroprevalence in rural zones of the state of Queretaro, Mexico, Am. J. Trop. Med. Hyg. 73 (2005) 510–516.
[39] P. Navarro, M. Sánchez-Moreno, C. Marín, E. García-España, F. Ramírez-Macías, F. Olmo, M.J. Rosales, F. Gómez-Contreras, M.J.R. Yunta, R. Gutierrez-Sánchez, *In vitro* leishmanicidal activity of pyrazole-containing polyamine macrocycles which inhibit the Fe-SOD enzyme of *Leishmania infantum* and *Leishmania.braziliensis* species, Parasitology 141 (2014) 1031–1043.
[40] A.F. Miller, D.L. Sorkin, K. Padmakumar, Anion binding properties of reduced and oxidized iron-containing superoxide dismutase reveal no requirement for Tyrosine 34, Biochemistry 44 (2005) 5969–5981.
[41] E. Yikilmaz, D.W. Rodgers, A.F. Miller, The crucial importance of chemistry in the structure-function link: manipulating hydrogen bonding in iron-containing superoxide dismutase, Biochemistry 45 (2006) 1151–1161.
[42] (a) C.K. Vance, A.F. Miller, Specificity and phenetic relationships of iron- and manganese-containing superoxide dismutases on the basis of structure and sequence comparisons, Biochemistry 40 (2001) 13079–13087;
(b) E. Yikilmaz, J. Xie, T.C. Brunold, A.F. Miller, Hydrogen-bond-mediated tuning of the redox potential of the non-heme Fe site of superoxide dismutase, J. Am. Chem. Soc. 124 (2002) 3482–3483;
(c) C.K. Vance, A.F. Miller, A simple proposal that can explain the inactivity of metal-substituted superoxide dismutases, J. Am. Chem. Soc. 120 (1998) 461–467;
(d) W.C. Stallings, A.L. Metzger, K.A. Pattridge, J.A. Fee, M.L. Ludwig, Structure-function relationships in iron and manganese superoxide dismutases, Free Radic. Res. Commun. 12–13 (1991) 259–268;
(e) W.G. Han, T. Lovell, L. Noodleman, Coupled redox potentials in manganese and iron superoxide dismutases from reaction kinetics and density functional/electrostatics calculation, Inorg. Chem. 41 (2002) 205–218.
[43] I.G. Muñoz, J.F. Moran, M. Becana, G. Montoya, The crystal structure of a eukaryotic iron superoxide dismutase suggests intersubunit cooperation during catalysis, Protein Sci. 14 (2005) 387–394.
[44] C.F. Da Silva, M.M. Batista, D.G.J. Batista, E.M. de Souza, P.B. da Silva, G.M. de Oliveira, A.S. Meuser, A.R. Shareef, D.W. Boykin, M.N.C. Soeiro, In vitro and in vivo studies of the trypanocidal activity of a diarylthiophene diamidine against *Trypanosoma cruzi*, Antimicrob. Agents Chemother. 9 (2008) 3307–3314.
[45] J.R. Coura, S.L. de Castro, A critical review on Chagas disease chemotherapy, Mem. Inst. Oswaldo Cruz 97 (2002) 3–24.
[46] J. Rivera, L.D. Hillis, B.D. Levine, Reactivation of cardiac Chagas disease in acquired immune deficiency syndrome, Am. J. Cardiol. 94 (2004) 1102–1103.
[47] S. Caldas, F.M. Santos, M. de Lana, L.F. Diniz, G.L. Machado-Coelho, V.M. Veloso, M.T. Bahia, *Trypanosoma cruzi*: acute and long-term infection in the vertebrate host can modify the response to benznidazole, Exp. Parasitol. 118 (3) (2008) 315–323.
[48] A. Bouhdidi, C. Truyens, M.T. Rivera, H. Bazin, Y. Carlier, *Trypanosoma cruzi* infection in mice induces a polyisotypic hypergammaglobulinaemia and parasite-specific response involving high IgG2a concentrations and highly avid IgG1 antibodies, Parasite Immunol. 16 (1994) 69–76.
[49] K.L. Cummings, R.L. Tarleton, Rapid quantitation of *Trypanosoma cruzi* in host tissue by real-time PCR, Mol. Biochem. Parasitol. 104 (2003) 53–59.